





Cite this: *RSC Adv.*, 2019, 9, 36808

# Selective separation of Xe/Kr and adsorption of water in a microporous hydrogen-bonded organic framework†

Wang-Geun Lee, <sup>a</sup> Tae-Ung Yoon,<sup>b</sup> Youn-Sang Bae, <sup>\*b</sup> Kwang S. Kim <sup>\*a</sup> and Seung Bin Baek <sup>\*a</sup>

We have studied the adsorption properties of Xe and Kr in a highly microporous hydrogen-bonded organic framework based on 1,3,5-tris(4-carboxyphenyl)benzene, named HOF-BTB. HOF-BTB can reversibly adsorb both noble gases, and it shows a higher affinity for Xe than Kr. At 1 bar, the adsorption amounts of Xe were 3.37 mmol g<sup>-1</sup> and 2.01 mmol g<sup>-1</sup> at 273 K and 295 K, respectively. Ideal adsorbed solution theory (IAST) calculation predicts selective separation of Xe over Kr from an equimolar binary Xe/Kr mixture, and breakthrough experiments demonstrate the efficient separation of Xe from the Xe/Kr mixture under a dynamic flow condition. Consecutive breakthrough experiments with simple regeneration treatment at 298 K reveal that HOF-BTB would be an energy-saving adsorbent in an adsorptive separation process, which could be attributed to the relatively low isosteric heat ( $Q_{st}$ ) of adsorption of Xe. The activated HOF-BTB is very stable in both water and aqueous acidic solutions for more than one month, and it also shows a well-preserved crystallinity and porosity upon water/acid treatment. Besides, HOF-BTB adsorbs about 30.5 wt%, the highest value for HOF materials, of water vapor during the adsorption–desorption cycles, with a 19% decrease in adsorption amounts of water vapor after five cycles.

Received 9th October 2019  
Accepted 5th November 2019

DOI: 10.1039/c9ra08184d

rsc.li/rsc-advances

## 1. Introduction

Hydrogen-bonded organic frameworks (HOFs) are a new class of porous crystalline material purely composed of multiple hydrogen bonding interactions and other non-covalent interactions like  $\pi$ – $\pi$  stacking.<sup>1,2</sup> Compared to coordination or covalent bonds, the hydrogen bond is generally weak and reversible, resulting in low rigidity. Nevertheless, the synergistic effect of multiple hydrogen bonding and  $\pi$ – $\pi$  stacking between organic linkers in the HOF's building unit makes it stable even after the removal of guest solvent molecules or even in an aqueous environment.<sup>3,4</sup> Over the past decade, they have attracted increasing interest with their applications including gas adsorption and separation,<sup>5–8</sup> proton conduction,<sup>9</sup> and sensing.<sup>10</sup>

After the first discovery of Kr and Xe in the late 19th century, the exploitation of these 'noble' gases has widely expanded from small bulbs, display, and laser industry to state-of-art

machinery, medical instruments, and space industry.<sup>11,12</sup> However, their production technique still stays in the conventional cryogenic method, which consumes much energy to cool down both gases in the air. Utilizing porous materials has been suggested as one of the effective ways to separate Xe from Kr.<sup>13,14</sup> Hence, selective adsorption/separation properties for various porous materials including charcoal, zeolites, zeolitic imidazolate frameworks (ZIFs), metal–organic frameworks (MOFs), and covalent organic frameworks (COFs)<sup>15–21</sup> have been reported to date. For example, Ag@MOF-74-Ni showed a remarkable ability to separate Xe from Kr.<sup>21</sup> For inert gas separation in metal-free materials, mostly considered factors are uniformity of the pore structure and pore size adjusted for Xe or Kr atom.<sup>22–24</sup> These factors predominantly affect the adsorption properties in porous carbons, COFs, organic cage, and even in several MOFs. For example, metal-free porous materials, such as activated carbon, CC3 (organic cages), and IISERP-POFs (porous organic frameworks), have shown quite comparable or even better Xe/Kr absorptivity and selectivity than MOFs.<sup>15,20,25</sup> In our previous work, we reported the highly microporous HOF material based on 1,3,5-tris(4-carboxyphenyl) benzene, named HOF-BTB,<sup>8</sup> which showed efficient selective separations of C<sub>2</sub> hydrocarbon/CH<sub>4</sub> binary gas mixtures in HOF-BTB. This selective separation is mainly due to strong van der Waals interaction between HOF-BTB and C<sub>2</sub> hydrocarbons. Since van der Waals interaction between the framework of HOF-

<sup>a</sup>Department of Chemistry, Ulsan National Institute of Science and Technology (UNIST), 50 UNIST-gil, Ulsan 44919, Republic of Korea. E-mail: kimks@unist.ac.kr; sbbaek@unist.ac.kr

<sup>b</sup>Department of Chemical and Biomolecular Engineering, Yonsei University, 50 Yonsei-ro, Seodaemun-gu, Seoul 03722, Republic of Korea. E-mail: mowbae@yonsei.ac.kr

† Electronic supplementary information (ESI) available: Virial fitting data of isotherms, additional PXRD and adsorption data. See DOI: 10.1039/c9ra08184d



BTB and noble gases is expected to be the most crucial factor for adsorption,<sup>26,27</sup> the results suggest that HOF-BTB would be a useful candidate for selective separation of noble gas mixtures.

Adsorption of water vapor is another important topic in an environmental or industrial area. In dry regions, the study for collecting fresh water at the low humidity level is much in demand. On the other hand, in manufacturing devices that are moisture-sensitive, a small amount of vapor or water could interrupt the proper operation.<sup>28</sup> To achieve practical progress in water harvest or humidity control, porous materials have been studied as adsorbents due to their potential for high working capacity. Several computational screenings and experiments on carbon materials, MOFs, and COFs show that MOF-801 and mesoporous MOF Co<sub>2</sub>Cl<sub>2</sub>(BTDD) gave an impressive performance under desert conditions.<sup>28–33</sup> For most porous materials, however, water stability is a challenging problem because their structures are occasionally deformed to lose their functionalities under moisture, resulting in the limitation in practical applications.<sup>34,35</sup> Especially MOFs with open metal sites suffered from water adsorption, and quite a number of MOFs having good performance are still facing huddles with water sensitivity.<sup>16,21,23,36</sup> Interestingly, several HOFs are known to be more durable than MOFs and COFs in a humid environment or even in water.<sup>7,10,37–40</sup> However, the study on water vapor adsorption in HOFs remains rare.

Herein, we report single-component adsorption–desorption properties of both Xe and Kr in the microporous HOF-BTB. The adsorption amounts of Xe is comparable to most reported MOFs and porous organic materials. Breakthrough experiments of an equimolar binary mixture of Xe/Kr reveal that HOF-BTB selectively separates Xe from Kr under a dynamic mixture flow condition. To the best of our knowledge, this study provides the first example of selective separation of Xe from Kr in HOF materials. Besides, HOF-BTB not only is very stable in both water and aqueous acidic solutions for more than one month but also shows a maximum adsorption capacity of about 30.5 wt% for water vapor during the adsorption–desorption cycles. More interestingly, it preserves crystallinity and permanent porosity even after the adsorption of water vapor. These results suggest that HOF-BTB would be a promising candidate for real-world application in effective dehydration under ambient conditions.

## 2. Experimental section

### 2.1 General considerations

HOF-BTB was synthesized as the previous report.<sup>8</sup> All chemicals were purchased and used without additional purification. 1,3,5-tris(4-carboxyphenyl)benzene (H<sub>3</sub>BTB) was dissolved in *N,N*-dimethylformamide (DMF) in a hot oven, and cooled down in a refrigerator to get H<sub>3</sub>BTB-DMF crystals. After decanting the mother solution, these crystals were dried in air and then soaked into methanol. This methanol solution was heated in an oven at 50 °C, producing HOF-BTB crystals in 24 hours. All powder X-ray diffraction (PXRD) patterns were recorded by

a Bruker D2 Phaser diffractometer operated at 30 kV and 10 mA with a scan rate of 0.2 deg s<sup>−1</sup>.

### 2.2 Adsorption–desorption experiments

Adsorption–desorption isotherms of Xe and Kr were measured using the standard volumetric procedure on the BELSORP-Mini II adsorption measuring system (BEL Japan, Inc), which was equipped with a temperature control unit. For water vapor adsorption–desorption measurements, the standard volumetric procedure on the BELSORP-Max low-pressure gas adsorption measuring system (BEL Japan, Inc) was used. Adsorption–desorption cycles of water vapor were done without re-activation of the HOF-BTB sample between each run. At least 50 mg of the crystals were pretreated at 393 K under vacuum for 15 hours before adsorption measurements. All the adsorption data were manipulated by BEL-Master software provided by BEL Japan Inc.

### 2.3 Fitting of isotherms and ideal adsorbed solution theory calculations<sup>41–43</sup>

The parameters for ideal adsorbed solution theory (IAST) selectivity calculations were determined by fitting the pure single-component isotherms using the single-site Langmuir–Freundlich model, purely based on the best fit with highest adjusted *R*<sup>2</sup>-values. The single-site Langmuir–Freundlich equation is given as follows:

$$q = \frac{q_{\text{sat}} \times b \times p^{1/n}}{1 + b \times p^{1/n}} \quad (1)$$

where *n* represents the deviation from an ideal homogeneous surface. The parameters *q*<sub>sat</sub>, *b*, and *n* can be extracted by fitting the experimental adsorption isotherms (*q* versus *p*). They are then used to calculate IAST selectivity. The adsorption selectivity (*S*<sub>ads</sub>) for a binary gas mixture of components 1 and 2 is defined as:

$$S_{\text{ads}} = \frac{q_1/q_2}{p_1/p_2} \quad (2)$$

where *q<sub>i</sub>* is the molar loading of the species *i* and *p<sub>i</sub>* is the partial pressure of species *i*. The integrals were computed at the website <http://integrals.wolfram.com>, and the adsorbed phase composition that minimized the difference between the integrals of the two spreading pressures was found at the website <http://www.wolframalpha.com>. Selectivities were then calculated according to eqn (2).

### 2.4 Breakthrough experiments

The breakthrough experiment of HOF-BTB for mixture gas separation was performed in a custom-built fixed bed equipment (Scheme S1†). The gas flow rates were regulated by three mass flow controllers (0–100 ml min<sup>−1</sup>) (Bronkhorst, Germany), where two of them were used for making combinations of Xe/Kr streams, and the last one was used for He stream. First, the He stream was used for the *in situ* regeneration of the adsorbent packed in the column, which is placed in a ventilated thermostatted oven for measurements at a constant temperature.



Secondly, the He flow was mixed with the Xe/Kr gas mixture to adjust the total pressure. A mass spectrometer (Extrel Max300-LG, USA) was used to measure the effluent gas composition from the column. The detailed description of breakthrough experimental setup and procedures can also be found elsewhere.<sup>44,45</sup> 500–1000  $\mu\text{m}$  of binderless HOF-BTB pellets was prepared by using a carver press (Carver, Inc., USA). These pellets were activated at 393 K for 15 hours under vacuum and then packed into a stainless-steel column (15 cm  $\times$  0.44 cm). The remainder of the column was filled with glass beads with a diameter of 750  $\mu\text{m}$ . Before the breakthrough experiments, the column was degassed by a He flow of 40 ml min<sup>-1</sup> at 393 K for 2 hours to remove all the impurities adsorbed during the packing procedure. All the experiments were carried out at 298 K and 1 bar. Before each measurement, a He flow of 40 ml min<sup>-1</sup> at 298 K was introduced into the column for at least 10 min. Simultaneously, a feed mixture for a breakthrough run was prepared as follows: a 20 ml min<sup>-1</sup> of He flow was combined with a 20 ml min<sup>-1</sup> of equimolar Xe/Kr and then mixed well with each other by flowing through a gas mixer. It should be noted that the obtained mixture can be considered as equimolar Xe/Kr at 0.5 bar. At  $t = 0$ , the He flow for *in situ* regeneration was stopped and the flow of the feed mixture was introduced into the packed column.

## 2.5 Computational methods

Geometry based analysis was conducted by Zeo++ (0.3 version) package.<sup>46–48</sup> To describe the pore structure or void structure of HOF-BTB, the crystal structure of HOF-BTB with P1 symmetry was used. Largest cavity diameter (LCD), pore limiting diameter (PLD), and channel dimensionality were calculated with a high accuracy setting, and an atomic radius was adopted from the Cambridge Crystallography Data Center (CCDC) as default. Probe radius of 1.4 Å was used for channel dimensionality calculation.

# 3. Results and discussion

## 3.1 Adsorption of Xe and Kr

HOF-BTB was prepared as the previous report, followed by thermal activation at 393 K for 15 hours in vacuum for gas adsorption experiments.<sup>8</sup> In order to evaluate the adsorption properties for noble gases, we performed the adsorption experiments for Xe and Kr at 273 K and 295 K up to 1 bar. Fig. 1a shows their adsorption-desorption isotherms at both temperatures. All adsorption isotherms are fully reversible in HOF-BTB, indicating that the physisorption process may govern the adsorption of both gases in HOF-BTB. At 1 bar of Xe pressure, HOF-BTB can take up 3.37 mmol g<sup>-1</sup> and 2.01 mmol g<sup>-1</sup> of Xe gas at 273 K and 295 K, respectively. These Xe uptakes are found to be comparable with those of carbon-based porous materials such as CC3 (2.4 mmol g<sup>-1</sup>, 295 K) and IISERP-POF8 (1.72 mmol g<sup>-1</sup>, 298 K).<sup>20,25</sup> Compared with MOFs, its uptake amounts of Xe is considerably lower than those of MOFs with active open-metal sites, such as Ni-MOF-74 (3.6–4.8 mmol g<sup>-1</sup>).<sup>15,21</sup> However, HOF-BTB adsorbs Xe as much as other representative

MOFs without open-metal sites, such as Co<sub>3</sub>(HCCO)<sub>6</sub> (2 mmol g<sup>-1</sup>), IRMOF-1 (2 mmol g<sup>-1</sup>) and CROFOUR-1-Ni (1.8 mmol g<sup>-1</sup>).<sup>49–52</sup> In contrast to the Xe uptakes, Kr uptake capacities of HOF-BTB are far less than those of Xe at both temperatures, with the values of 0.672 mmol g<sup>-1</sup> and 0.416 mmol g<sup>-1</sup> at 273 K and 295 K, respectively. Higher adsorption of Xe in HOF-BTB could be attributed to the larger polarizability of Xe compared to Kr,<sup>22,36,51,53</sup> resulting in the higher affinity of Xe to the surfaces of BTB-HOF. Fig. 1b shows loading dependent isosteric heats ( $Q_{\text{st}}$ ) of adsorption calculated based on adsorption isotherms at 273 K and 295 K by using the virial method (Fig. S1 and S2†). The loading dependent  $Q_{\text{st}}$  of Xe is larger than that of Kr, which indicates that the stronger interaction between Xe and the pore surfaces of HOF-BTB than that of Kr and HOF-BTB. For both gases, the values of  $Q_{\text{st}}$  remain almost constant through the whole loading ranges. Thus, the pore surface of HOF-BTB is considered to be homogeneous. The  $Q_{\text{st}}$  value of Xe at zero limit surface coverage is estimated to be 18.7 kJ mol<sup>-1</sup>, which falls in the ideal range (*i.e.*, 17.5 to 35 kJ mol<sup>-1</sup>) for efficient separation of Xe/Kr mixture proposed by Tong and coworkers.<sup>19</sup> For Kr adsorption, the  $Q_{\text{st}}$  of Kr is calculated to be 14.3 kJ mol<sup>-1</sup>, lower than that of Xe, indicative of weaker binding of Kr than Xe in HOF-BTB.

To analyze the selective separation ability of Xe from binary Xe/Kr mixture, the pure single-component isotherms of Xe and Kr were fitted with the Langmuir-Freundlich isotherm model (Fig. S3–S6†).<sup>42</sup> Then, we used ideal adsorbed solution theory (IAST)<sup>43</sup> to predict the separation selectivity of binary Xe/Kr gas mixture (50 : 50) at 273 K and 295 K. The IAST calculation predicts that HOF-BTB could allow selective separation of Xe over Kr from the binary Xe/Kr gas mixture. Fig. 2a shows the IAST-predicted Xe/Kr selectivity up to 1 bar of total gas pressures at 273 K and 295 K. Since the IAST prediction on the gas mixture behavior is based on the adsorption equilibrium, it cannot reflect the mixture behavior in terms of adsorption kinetics. Hence, we carried out dynamic breakthrough experiments to evaluate the potential of HOF-BTB for the adsorptive separation of Xe/Kr mixture under dynamic flow conditions. Fig. 2b shows experimental breakthrough curves of Xe/Kr mixture on a column packed with HOF-BTB pellets at 298 K. Kr gas elutes first from the column, whereas Xe is retained in the column. This indicates that HOF-BTB primarily adsorbs Xe rather than Kr, resulting in efficient separation of Xe over Kr under dynamic flow conditions. Energy-saving regeneration of the used adsorbent is an important factor for the practical operation of an adsorptive separation process. After performing a breakthrough experiment, we regenerated the column by simply purging it for 10 min under a He flow of 40 ml min<sup>-1</sup> at 298 K. As displayed in Fig. 2b, essentially identical breakthrough curves were obtained during the three consecutive cycles, which is remarkable because the regenerations were performed under mild conditions without heating the column. This energy-saving regeneration condition could be attributed to the relatively small  $Q_{\text{st}}$  value for Xe adsorption. To the best of our knowledge, this is the first example of selective separation of Xe from Kr in HOF materials.



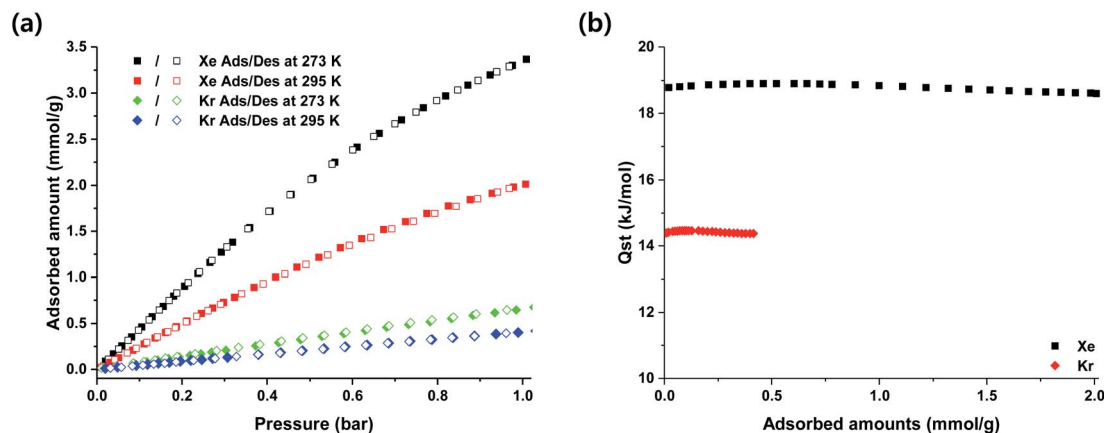


Fig. 1 (a) Xe and Kr adsorption–desorption isotherms at 273 K and 295 K. (b) Loading dependent isosteric heat ( $Q_{st}$ ) of adsorption for Xe and Kr. The  $Q_{st}$  were calculated from adsorption isotherms obtained at 273 K and 295 K by the virial method.

Further studies on the channel structure were carried out to understand adsorption behavior and selectivity of HOF-BTB. For Xe/Kr selectivity, characteristics of the pore structure are known to be one of the crucial factors. Thus, we calculated the largest cavity diameter (LCD) and pore limiting diameter (PLD) of HOF-BTB using open source Zeo++ code (0.3 version).<sup>46,47</sup> LCD and PLD of HOF-BTB were estimated to be 9.80 Å and 5.93 Å, respectively. Both void structure and LCD/PLD calculation showed that HOF-BTB has one type of one-dimensional channels, with 5.93 Å of the narrowest diameter along the channel path to 9.80 Å of the widest diameter along the channel path. According to Sikora *et al.*, the ratio of LCD/PLD correlates with Xe/Kr selectivity: the lower ratio of LCD/PLD (within 1 and 2, ideally 1), the higher Xe selectivity.<sup>23</sup> They also proposed that the LCDs should be within the range of 4.1 Å ~ 8.2 Å, corresponding to the 1–2 times of atomic Xe (4.1 Å), to achieve the effective separation selectivity of a Xe/Kr mixture. The calculated LCD/PLD ratio (1.65) of HOF-BTB falls in this range, and the calculated LCD value (9.80 Å) of HOF-BTB is a little larger than the upper limit (8.2 Å).

### 3.2 Stability in water and acid solutions

One of the challenging tasks of porous crystalline materials is to enhance stability to moisture. Some HOF materials have been reported to have higher stability under exposure to moisture or in water.<sup>38–40</sup> To evaluate the stability of HOF-BTB in the presence of water, we immersed as-prepared HOF-BTB crystals, as well as thermally activated crystals, into distilled water for a month. All observed PXRD patterns of both HOF-BTB crystals are in good agreement with the simulated PXRD pattern (Fig. 3a and S7†). The HOF-BTB crystals maintain crystallinity in water for three months. We further tested the stability of HOF-BTB crystals in three aqueous acidic solutions, 1 N solution of HCl, H<sub>2</sub>SO<sub>4</sub>, and H<sub>3</sub>PO<sub>4</sub>, respectively. Similarly, all observed PXRD patterns of HOF-BTB soaked in the acidic solutions for a month are well-matched with that of the as-prepared one (Fig. 3a), indicating that no significant deformation or destruction of crystal structures occurred in the acidic solutions for a month. To confirm a permanent porosity of activated HOF-BTB after water/acid treatment, we measured N<sub>2</sub> adsorption

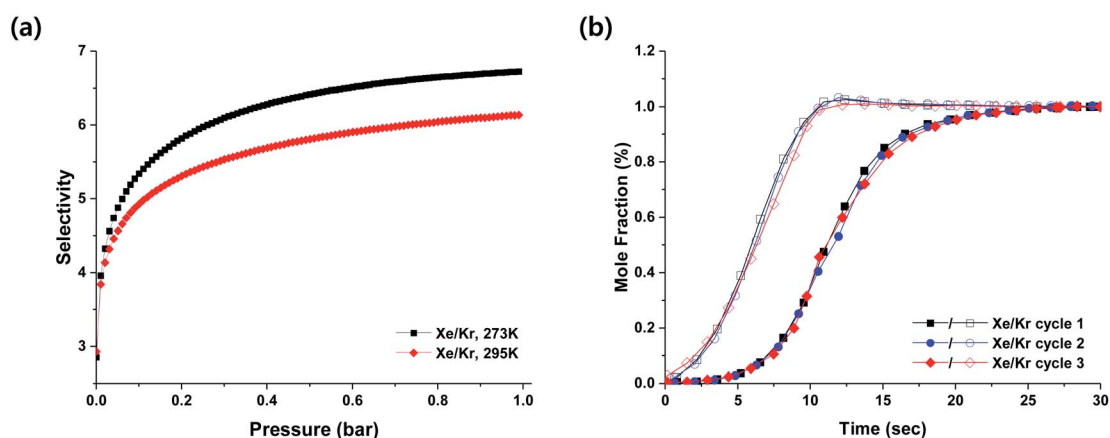


Fig. 2 (a) The IAST-predicted pressure dependent binary Xe/Kr mixture separation selectivity of HOF-BTB. (b) The experimental breakthrough curves at three consecutive cycles for a packed-bed filled with HOF-BTB pellets at 298 K. The total pressure of binary Xe/Kr mixture is 0.5 bar. For each run, 20 ml min<sup>−1</sup> of He flow was mixed with the equimolar mixture of Xe/Kr (20 ml min<sup>−1</sup>).



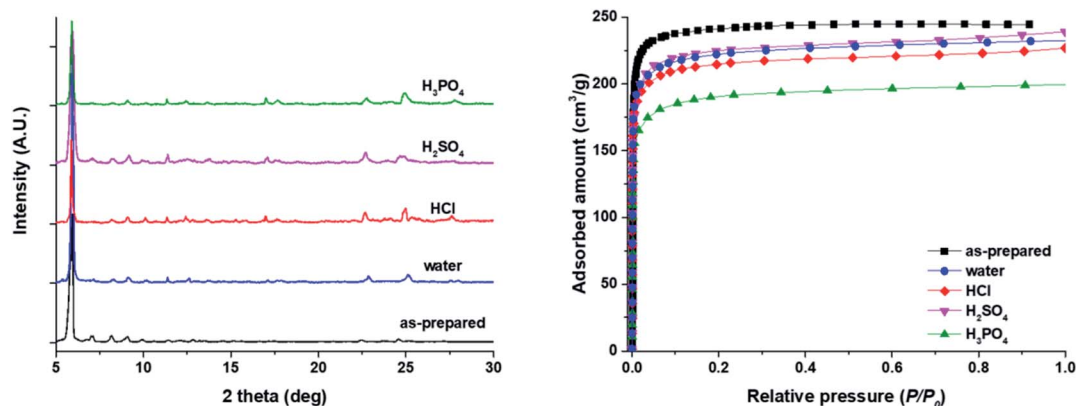


Fig. 3 (a) Powder X-ray diffraction patterns of activated HOF-BTB crystals after one month in water, 1 N HCl, 1 N H<sub>2</sub>SO<sub>4</sub>, and 1 N H<sub>3</sub>PO<sub>4</sub>. (b) N<sub>2</sub> adsorption isotherms at 77 K in water, 1 N HCl, 1 N H<sub>2</sub>SO<sub>4</sub>, and 1 N H<sub>3</sub>PO<sub>4</sub>, for one week.

isotherms at 77 K. While the specific surface area of activated HOF-BTB without any treatment is 1050 m<sup>2</sup> g<sup>-1</sup>, all the measured surface areas of activated HOF-BTB samples immersed in water, HCl, H<sub>2</sub>SO<sub>4</sub>, and H<sub>3</sub>PO<sub>4</sub> for a week decreased to 865 m<sup>2</sup> g<sup>-1</sup>, 846 m<sup>2</sup> g<sup>-1</sup>, 874 m<sup>2</sup> g<sup>-1</sup>, and 730 m<sup>2</sup> g<sup>-1</sup> (Fig. 3b). The decrease in the surface areas may be due to the partial collapse of the HOF-BTB frameworks in each solution. In water, after three months, activated HOF-BTB still preserves crystallinity (Fig. S8†). However, specific surface area of HOF-BTB decreased further to 816 m<sup>2</sup> g<sup>-1</sup> even after one month (Fig. S9†). In the case of activated HOF-BTB in the acid solutions, the residual ions in the pore might cause a decrease in the surface areas as well as the partial collapses of the frameworks.

### 3.3 Water vapor adsorption

Though some HOFs are known to have good water stability, water vapor adsorption properties of HOF materials have been rarely reported. Water vapor adsorption-desorption isotherms of HOF-BTB were depicted in Fig. 4a, for 298 K and 308 K. While HOF-BTB has no initial uptake of water vapor up to  $P/P_0 \approx 0.40$

at 298 K, it starts to adsorb water vapor above  $P/P_0 \approx 0.40$ . Similarly, the adsorption amount of water vapor is negligible less than  $P/P_0 \approx 0.40$  at 308 K. At  $P/P_0 = 0.9$ , HOF-BTB adsorbed 304.6 mg g<sup>-1</sup> of water vapor at 298 K and 252.2 mg g<sup>-1</sup> at 308 K. These water vapor uptakes of HOF-BTB is much higher than that of the recently reported porphyrin based HOF, TCPP-1,3-DPP (91 mg g<sup>-1</sup> at 298 K).<sup>40</sup> Though its uptake is smaller than that of representative porous materials such as MOF-808, Cr-MIL-101, MCM-41, TpBpy, and CPOP-9, it is comparable to materials with similar surface areas.<sup>54–57</sup> For example, NU-POP-1, CE-1, and MOF-801 P (with the surface area of 950 cm<sup>3</sup> g<sup>-1</sup>, 960 cm<sup>3</sup> g<sup>-1</sup>, and 990 cm<sup>3</sup> g<sup>-1</sup>, respectively) showed uptakes of 230 mg g<sup>-1</sup>, 220 mg g<sup>-1</sup>, and 362 mg g<sup>-1</sup>, respectively.<sup>54,58,59</sup> The adsorption isotherm is type V, with a negligible hysteresis loop. The steep inflection point appeared at  $P/P_0 \approx 0.45$  for both temperatures, indicating that HOF-BTB has hydrophobic nature, which would be originated from the contribution of aromatic rings in the H<sub>3</sub>BTB ligand. Small hysteresis could be explained with micropore characteristics of HOF-BTB.<sup>60</sup> The steep increase in the water uptake within a narrow range is regarded as the desired feature for cyclic water harvesting. In

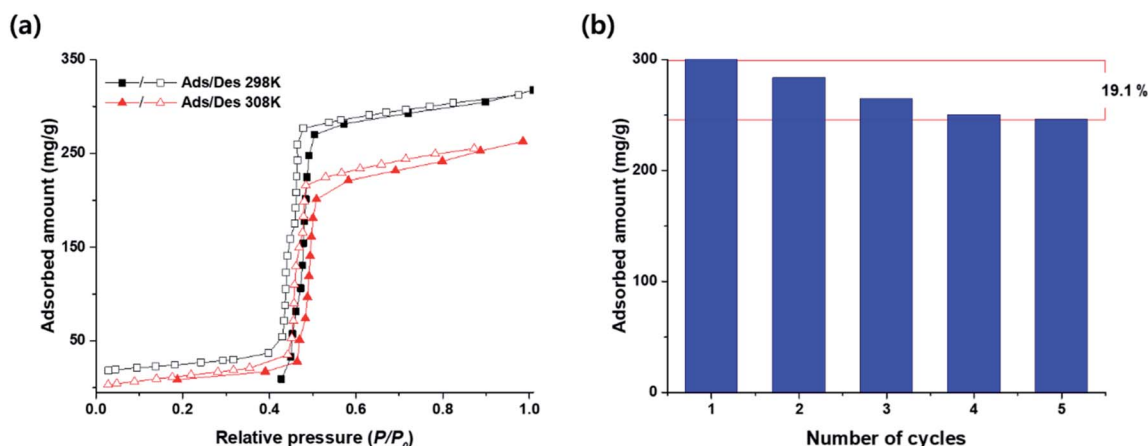


Fig. 4 (a) Adsorption-desorption isotherms of water vapor in activated HOF-BTB crystals, at 298 K and 308 K. (b) Adsorption-desorption cycles for activated HOF-BTB, both adsorption and desorption at 298 K.



terms of energy efficiency, reversible adsorption–desorption of water vapor, without any hysteresis within a narrow range of  $P/P_0$ , is energetically favorable for application in water harvesting.<sup>32</sup>

To evaluate its durability and stability upon water adsorption–desorption cycles, we conducted five consecutive adsorption–desorption cycles at 298 K. At every cycle, the adsorption amount of water gradually decreased, but it shows almost the same adsorption amounts in the fourth and fifth cycles (Fig. 4b). After the fifth cycle, HOF-BTB could adsorb 80.9% of the adsorption amount of the first cycle, unlike MOF-808 or MOF-74 that showed drastically decreased uptakes after the fifth cycle.<sup>54</sup> All isotherms obtained at each adsorption–desorption cycle show the reversible type V, without changing the inflection point (Fig. S10†). Along with long term stability in water and aqueous acid solutions, this cyclable water adsorption properties of HOF-BTB would be an advantageous aspect for industrial use.

## 4. Conclusions

We have studied the adsorption properties of Xe and Kr in a highly microporous HOF-BTB. HOF-BTB reversibly adsorbs Xe and Kr with a higher affinity for Xe than Kr. The small isosteric heats of adsorption indicate that the physisorption is likely to govern the adsorption of Xe and Kr in HOF-BTB. As predicted by IAST, the breakthrough experiments reveal that HOF-BTB can selectively separate Xe over Kr from the equimolar binary mixture of Xe/Kr under a dynamic flow condition. Furthermore, easy regeneration of the column packed with HOF-BTB at 298 K without loss of separation selectivity during the consecutive breakthrough experiments indicates that HOF-BTB would be an energy-saving adsorbent in an adsorptive separation process. The activated HOF-BTB is very stable in both water and aqueous acidic solutions for more than one month, and it also shows a well-preserved crystallinity and porosity upon water/acid treatment. Besides, HOF-BTB can adsorb water vapor during the adsorption–desorption cycles. We anticipate that HOF-BTB will become the promising and energetically favorable adsorbent in applications relating to dehydration processes.

## Conflicts of interest

There are no conflicts to declare.

## Acknowledgements

This work was supported by Basic Science Research Program through the National Research Foundation of Korea (NRF) funded by the Ministry of Education (2019R11A1A01062148). This research was also supported by Human Resources Program in Energy Technology of the Korea Institute of Energy Technology Evaluation and Planning (KETEP), granted financial resource from the Ministry of Trade, Industry & Energy, Republic of Korea (no. 20174010201640).

## Notes and references

- 1 R.-B. Lin, Y. He, P. Li, H. Wang, W. Zhou and B. Chen, *Chem. Soc. Rev.*, 2019, **48**, 1362–1389.
- 2 K. S. Kim, P. Tarakeshwar and J. Y. Lee, *Chem. Rev.*, 2000, **100**, 4145–4185.
- 3 J. Luo, J.-W. Wang, J.-H. Zhang, S. Lai and D.-C. Zhong, *CrystEngComm*, 2018, **20**, 5884–5898.
- 4 I. Hisaki, Y. Suzuki, E. Gomez, Q. Ji, N. Tohnai, T. Nakamura and A. Douhal, *J. Am. Chem. Soc.*, 2019, **141**, 2111–2121.
- 5 C. A. Zentner, H. W. H. Lai, J. T. Greenfield, R. A. Wisconsin, M. Zeller, C. F. Campana, O. Talu, S. A. FitzGerald and J. L. C. Rowsell, *Chem. Commun.*, 2015, **51**, 11642–11645.
- 6 H. Wang, B. Li, H. Wu, T.-L. Hu, Z. Yao, W. Zhou, S. Xiang and B. Chen, *J. Am. Chem. Soc.*, 2015, **137**, 9963–9970.
- 7 F. Hu, C. Liu, M. Wu, J. Pang, F. Jiang, D. Yuan and M. Hong, *Angew. Chem., Int. Ed.*, 2017, **56**, 2101–2104.
- 8 T.-U. Yoon, S. B. Baek, D. Kim, E.-J. Kim, W.-G. Lee, B. K. Singh, M. S. Lah, Y.-S. Bae and K. S. Kim, *Chem. Commun.*, 2018, **54**, 9360–9363.
- 9 A. Karmakar, R. Illathvalappil, B. Anothumakkool, A. Sen, P. Samanta, A. V. Desai, S. Kurungot and S. K. Ghosh, *Angew. Chem., Int. Ed.*, 2016, **55**, 10667–10671.
- 10 Q. Yin, P. Zhao, R.-J. Sa, G.-C. Chen, J. Lü, T.-F. Liu and R. Cao, *Angew. Chem., Int. Ed.*, 2018, **57**, 7691–7696.
- 11 S. C. Cullen and E. G. Gross, *Science*, 1951, **113**, 580–582.
- 12 T. F. Holsträter, M. Georgieff, K. J. Föhr, W. Klingler, M. E. Uhl, T. Walker, S. Köster, G. Grön and O. Adolph, *Anesthesiology*, 2011, **115**, 398–407.
- 13 D. Banerjee, A. J. Cairns, J. Liu, R. K. Motkuri, S. K. Nune, C. A. Fernandez, R. Krishna, D. M. Strachan and P. K. Thallapally, *Acc. Chem. Res.*, 2015, **48**, 211–219.
- 14 U. Mueller, M. Schubert, F. Teich, H. Puetter, K. Schierle-Arndt and J. Pastré, *J. Mater. Chem.*, 2006, **16**, 626–636.
- 15 J. Liu, P. K. Thallapally and D. Strachan, *Langmuir*, 2012, **28**, 11584–11589.
- 16 P. K. Thallapally, J. W. Grate and R. K. Motkuri, *Chem. Commun.*, 2012, **48**, 347–349.
- 17 W. D. Machin, *J. Chem. Soc., Faraday Trans.*, 1992, **88**, 729–735.
- 18 M. Tong, Y. Lan, Q. Yang and C. Zhong, *Chem. Eng. Sci.*, 2017, **168**, 456–464.
- 19 J. A. Greathouse, T. L. Kinnibrugh and M. D. Allendorf, *Ind. Eng. Chem. Res.*, 2009, **48**, 3425–3431.
- 20 L. Chen, P. S. Reiss, S. Y. Chong, D. Holden, K. E. Jelfs, T. Hasell, M. A. Little, A. Kewley, M. E. Briggs, A. Stephenson, K. M. Thomas, J. A. Armstrong, J. Bell, J. Busto, R. Noel, J. Liu, D. M. Strachan, P. K. Thallapally and A. I. Cooper, *Nat. Mater.*, 2014, **13**, 954–960.
- 21 J. Liu, D. M. Strachan and P. K. Thallapally, *Chem. Commun.*, 2014, **50**, 466–468.
- 22 K. Vellingiri, K.-H. Kim, A. Pournara and A. Deep, *Prog. Mater. Sci.*, 2018, **94**, 1–67.
- 23 B. J. Sikora, C. E. Wilmer, M. L. Greenfield and R. Q. Snurr, *Chem. Sci.*, 2012, **3**, 2217.



- 24 D. Banerjee, C. M. Simon, A. M. Plonka, R. K. Motkuri, J. Liu, X. Chen, B. Smit, J. B. Parise, M. Haranczyk and P. K. Thallapally, *Nat. Commun.*, 2016, **7**, ncomms11831.
- 25 D. Chakraborty, S. Nandi, M. A. Sinnwell, J. Liu, R. Kushwaha, P. K. Thallapally and R. Vaidhyanathan, *ACS Appl. Mater. Interfaces*, 2019, **11**, 13279–13284.
- 26 M. Miklitz, S. Jiang, R. Clowes, M. E. Briggs, A. I. Cooper and K. E. Jelfs, *J. Phys. Chem. C*, 2017, **121**, 15211–15222.
- 27 R. S. Patil, D. Banerjee, C. M. Simon, J. L. Atwood and P. K. Thallapally, *Chem.–Eur. J.*, 2016, **22**, 12618–12623.
- 28 Y. Byun, S. H. Je, S. N. Talapaneni and A. Coskun, *Chem.–Eur. J.*, 2019, **25**, 10262–10283.
- 29 J. Canivet, A. Fateeva, Y. Guo, B. Coasne and D. Farrusseng, *Chem. Soc. Rev.*, 2014, **43**, 5594–5617.
- 30 L. Liu, S. Tan, T. Horikawa, D. D. Do, D. Nicholson and J. Liu, *Adv. Colloid Interface Sci.*, 2017, **250**, 64–78.
- 31 N. C. Burtch, H. Jasuja and K. S. Walton, *Chem. Rev.*, 2014, **114**, 10575–10612.
- 32 H. Kim, S. Yang, S. R. Rao, S. Narayanan, E. A. Kapustin, H. Furukawa, A. S. Umans, O. M. Yaghi and E. N. Wang, *Science*, 2017, **356**, 430–434.
- 33 A. J. Rieth, S. Yang, E. N. Wang and M. Dincă, *ACS Cent. Sci.*, 2017, **3**, 668–672.
- 34 J. Duan, W. Jin and S. Kitagawa, *Coord. Chem. Rev.*, 2017, **332**, 48–74.
- 35 J. J. Low, A. I. Benin, P. Jakubczak, J. F. Abrahamian, S. A. Faheem and R. R. Willis, *J. Am. Chem. Soc.*, 2009, **131**, 15834–15842.
- 36 J. J. Perry, S. L. Teich-McGoldrick, S. T. Meek, J. A. Greathouse, M. Haranczyk and M. D. Allendorf, *J. Phys. Chem. C*, 2014, **118**, 11685–11698.
- 37 X. Z. Luo, X. J. Jia, J. H. Deng, J. L. Zhong, H. J. Liu, K. J. Wang and D. C. Zhong, *J. Am. Chem. Soc.*, 2013, **135**, 11684–11687.
- 38 W. Yang, J. Wang, H. Wang, Z. Bao, J. C.-G. Zhao and B. Chen, *Cryst. Growth Des.*, 2017, **17**, 6132–6137.
- 39 I. Hisaki, N. Ikenaka, E. Gomez, B. Cohen, N. Tohnai and A. Douhal, *Chem.–Eur. J.*, 2017, **23**, 11611–11619.
- 40 Y. Luo, X. He, D. Hong, C. Chen, F. Chen, J. Jiao, L. Zhai, L. Guo and B. Sun, *Adv. Funct. Mater.*, 2018, **28**, 1804822.
- 41 J. M. Simmons, H. Wu, W. Zhou and T. Yildirim, *Energy Environ. Sci.*, 2011, **4**, 2177–2185.
- 42 J. A. Mason, K. Sumida, Z. R. Herm, R. Krishna and J. R. Long, *Energy Environ. Sci.*, 2011, **4**, 3030–3040.
- 43 Z. R. Herm, J. A. Swisher, B. Smit, R. Krishna and J. R. Long, *J. Am. Chem. Soc.*, 2011, **133**, 5664–5667.
- 44 S.-J. Lee, K. C. Kim, T.-U. Yoon, M.-B. Kim and Y.-S. Bae, *Microporous Mesoporous Mater.*, 2016, **236**, 284–291.
- 45 S.-J. Lee, T.-U. Yoon, A.-R. Kim, S.-Y. Kim, K.-H. Cho, Y. K. Hwang, J.-W. Yeon and Y.-S. Bae, *J. Hazard. Mater.*, 2016, **320**, 513.
- 46 T. F. Willems, C. H. Rycroft, M. Kazi, J. C. Meza and M. Haranczyk, *Microporous Mesoporous Mater.*, 2012, **149**, 134–141.
- 47 R. L. Martin, B. Smit and M. Haranczyk, *J. Chem. Inf. Model.*, 2012, **52**, 308–318.
- 48 M. Pinheiro, R. L. Martin, C. H. Rycroft and M. Haranczyk, *CrystEngComm*, 2013, **15**, 7531.
- 49 K. V. Lawler, Z. Hulvey and P. M. Forster, *Chem. Commun.*, 2013, **49**, 10959.
- 50 H. Wang, K. Yao, Z. Zhang, J. Jagiello, Q. Gong, Y. Han and J. Li, *Chem. Sci.*, 2014, **5**, 620–624.
- 51 S. T. Meek, S. L. Teich-McGoldrick, J. J. Perry, J. A. Greathouse and M. D. Allendorf, *J. Phys. Chem. C*, 2012, **116**, 19765–19772.
- 52 M. H. Mohamed, S. K. Elsaidi, T. Pham, K. A. Forrest, H. T. Schaefer, A. Hogan, L. Wojtas, W. Xu, B. Space, M. J. Zaworotko and P. K. Thallapally, *Angew. Chem., Int. Ed.*, 2016, **55**, 8285–8289.
- 53 R. Anderson, B. Schweitzer, T. Wu, M. A. Carreon and D. A. Gómez-Gualdrón, *ACS Appl. Mater. Interfaces*, 2018, **10**, 582–592.
- 54 H. Furukawa, F. Gándara, Y.-B. Zhang, J. Jiang, W. L. Queen, M. R. Hudson and O. M. Yaghi, *J. Am. Chem. Soc.*, 2014, **136**, 4369–4381.
- 55 S. Karak, S. Kandambeth, B. P. Biswal, H. S. Sasmal, S. Kumar, P. Pachfule and R. Banerjee, *J. Am. Chem. Soc.*, 2017, **139**, 1856–1862.
- 56 J. Ehrenmann, S. K. Henninger and C. Janiak, *Eur. J. Inorg. Chem.*, 2011, **2011**, 471–474.
- 57 Q. Chen, D.-P. Liu, J.-H. Zhu and B.-H. Han, *Macromolecules*, 2014, **47**, 5926–5931.
- 58 G. W. Peterson, O. K. Farha, B. Schindler, P. Jones, J. Mahle and J. T. Hupp, *J. Porous Mater.*, 2012, **19**, 261–266.
- 59 H. Yu, C. Shen, M. Tian, J. Qu and Z. Wang, *Macromolecules*, 2012, **45**, 5140–5150.
- 60 M. Nakamura, T. Ohba, P. Branton, H. Kanoh and K. Kaneko, *Carbon*, 2010, **48**, 305–308.

